

## Article

# Numerical Analysis of Hydrodynamic Loads on Passing and Moored Ships in Shallow Water

Ji-Yong Park <sup>1,2</sup>, Bo Woo Nam <sup>2,\*</sup> and Yonghwan Kim <sup>2</sup>

<sup>1</sup> Korean Research Institute of Ship & Ocean Engineering, Yuseong-Daero 1312 Beon-Gil, Yuseong-Gu, Daejeon 34103, Korea; jypark@kriso.re.kr

<sup>2</sup> Department of Naval Architecture and Ocean Engineering, Seoul National University, 1 Gwanak-Ro, Gwanak-Gu, Seoul 08826, Korea; yhwankim@snu.ac.kr

\* Correspondence: bwnam@snu.ac.kr

**Abstract:** In this study, hydrodynamic interactions between passing and moored ships were studied by applying a time-domain numerical simulation method. The boundary value problem for a fluid domain was formulated based on a potential flow theory. A numerical method was developed based on a finite element method with an efficient re-mesh algorithm. Regarding the free-surface boundary conditions, both double-body and free-surface models were considered for examining the free-surface effect on the hydrodynamic forces due to the passing ship. First, numerical results were validated by comparison with the model test results of Kriebel et al. (2005), where generic Series 60 hulls were considered as the target model for the passing and moored ships. In addition, hydrodynamic pressure fields and force time-series were investigated to understand the passing ship problem. Second, a series of numerical simulations were performed to study the effects of the passing ship speed, separation distance, water depth, and relative vessel size, which were used to compare the peak values of hydrodynamic forces. The applicability and limitations of the double-body and free-surface models are discussed for predicting passing ship loads.

**Keywords:** passing ship; hydrodynamic load; time-domain simulation; finite element method



**Citation:** Park, J.-Y.; Nam, B.W.; Kim, Y. Numerical Analysis of Hydrodynamic Loads on Passing and Moored Ships in Shallow Water. *Processes* **2021**, *9*, 558. <https://doi.org/10.3390/pr9030558>

Academic Editor:  
Krzysztof Rogowski

Received: 24 February 2021  
Accepted: 18 March 2021  
Published: 22 March 2021

**Publisher's Note:** MDPI stays neutral with regard to jurisdictional claims in published maps and institutional affiliations.



**Copyright:** © 2021 by the authors. Licensee MDPI, Basel, Switzerland. This article is an open access article distributed under the terms and conditions of the Creative Commons Attribution (CC BY) license (<https://creativecommons.org/licenses/by/4.0/>).

## 1. Introduction

In ports or coastal areas, an advancing ship is often observed to pass near moored or anchored ships. In particular, as the speed and size of ships have increased recently, the effect of large and high-speed passing ships has become an important consideration for the safety of moored ships. It is known that significant changes in the hydrodynamic pressure field around a passing ship can cause an excessive horizontal motion in moored ships, which, in turn, may result in collisions with other ships or the quay wall. For instance, in the worst-case scenario, damage to a berthing or offloading ship's mooring and mechanical equipment could result in a massive explosion and injuries [1]. Consequently, for the safe design of the mooring system of anchored vessels or the establishment of reasonable operating regulations—such as the passing ship speed and separation distance—computation and prediction methods for the effect of passing ship loads on a moored ship are necessary.

Researchers have conducted many model tests for the passing ship problem in order to understand the fundamental physics and directly measure the passing ship loads acting on a moored ship. Thus, various empirical formulas have been proposed based on model test results. Remery [2] conducted a 1:60 scale model test to examine a large tanker moored at an oil loading terminal in shallow water. Similarly, Muga [3] performed a 1:68 scale model test for supertankers and found that passing ship loads tend to increase with reduced separation distance or increased vessel speed or vessel size. Vantorre [4] conducted a 1:75 scale model test for a bulk carrier, container ship, and tanker and analyzed ship–ship interaction loads for encountering and overtaking cases. While previous experimental

studies on the passing ship problem were performed on specific ship models with limited variables, Kriebel [5] performed a 1:135 scale model test using a general Series 60 ship model with several variables, such as passing vessel speed, vessel displacement, water depth, and separation distance. Moreover, by analyzing these experimental results, Kriebel developed empirical equations and evaluated the applicability of the two existing models of Flory [6] and Seelig [7] on the passing ship problem. Swiegers [8] also conducted a 1:100 scale model test for a moored bulk carrier and a passing container ship using several variables such as the passing speed, separation distance, water depth, and presence of walls and channels.

In addition to the model test approach, researchers have also attempted to solve the passing ship problem by introducing semi-empirical formulas based on slender-body theory [7,9]. However, the application of two-dimensional (2D) numerical methods for three-dimensional (3D) vessels has limitations, and performing numerous model tests to identify empirical coefficients using various ship shapes and sizes is difficult. Accordingly, in the 2000s, 3D potential flow models considering detailed shape and the surrounding terrain features of ship were developed to establish a generalized prediction method for passing ship loads. Initially, Pinkster [10] adopted potential flow methods based on the boundary element method for low-speed passing ships and performed a comparative study by applying the double-body and free-surface models. The analysis of free-surface effects demonstrated the applicability of the double-body model for the passing ship problem compared to the free-surface model. However, in this study, the presence of the moored ship was not considered in the free-surface model, and the free-surface effect was not analyzed rigorously enough. Molen [11] also simulated the passing ship problem using the potential flow model based on the double-body flow assumption applied by Pinkster [10] and validated their numerical results against Swiegers' model test [8]. In his study, simulations of the passing ship problem in open water or with the presence of a quay wall or channel wall provided a good approximation of the model test results. Recently, unlike previous studies where numerous 3D potential flow models were applied based on the boundary element method, Nam [12] and Park [13] solved the passing ship problem using the classical finite element method (FEM). Nam [12] analyzed complex hydrodynamic interaction forces, including the presence of passing and moored ships and the influence of surrounding terrain features, such as the seabed and sidewall. He studied a relatively high-speed passing ship and a moored barge alongside a quay by varying the simulation parameters, such as the passing ship speed, wall distances, separation distance, and waves, including the free-surface effect.

Direct numerical simulations based on computational fluid dynamics (CFD) have also been applied for the passing ship problem. Huang [14] analyzed the influence of the passing ship layout, speed, and separation distance on vessels moored at piers using a Reynolds-averaged Navier–Stokes (RANS)-based CFD model. Wang [15] also used the unsteady RANS-based CFD model to analyze the hydrodynamic interaction that occurs in a single-way lock. These studies were conducted by applying an undisturbed free-surface boundary condition using the double-body model, but the free-surface effects were not considered. Recently, with the rapid development of the CFD technique and computational hardware, CFD simulations have been increasingly used to analyze the passing ship problem, including the effects of vorticity and viscosity in limited passing ship problem conditions. However, thus far, this method still requires enormous computational time and hardware costs compared to existing potential flow models, and additional verification procedures are needed for accurate and reliable CFD simulation results.

In this study, we investigated the passing ship problem in order to predict the hydrodynamic forces acting on a moored ship resulting from a passing ship. The computations were performed using the 3D potential flow model based on the classical FEM. Two types of free-surface boundary conditions were applied: the double-body and free-surface models. The computational results were compared with those of Kriebel's model test [5] for validation. Simulation parameters, such as the passing ship speed, separation distance,

and water depth, were analyzed using generic Series 60 hulls as the passing and moored ships. Moreover, the relative length, breadth, and draft of the moored ship were varied to investigate the influence of the vessel size.

## 2. Numerical Method

### 2.1. Boundary Value Problem

A numerical method based on 3D potential flow theory was developed for the computations of the passing ship problem. Here, an inviscid and incompressible fluid and an irrotational flow were assumed. Two numerical models, double-body and free-surface models, were applied to solve boundary value problems for the fluid domain. In the double-body model, the free surface is assumed as a rigid wall boundary under a low-speed condition of a passing ship, which was adopted by Korsmeyer [16] and Pinkster [10,17] for the passing ship problem. The boundary value problem of the double-body model is as follows (Figure 1):

$$\nabla^2 \phi = 0 \quad \text{in } \Omega(t) \quad (1)$$

$$\frac{\partial \phi}{\partial n} = \vec{n} \cdot \vec{U} \quad \text{on } \overline{S_{B1}}, \overline{S_{B2}} \quad (2)$$

$$\frac{\partial \phi}{\partial n} = 0 \quad \text{on } z = 0, z = -h \quad (3)$$

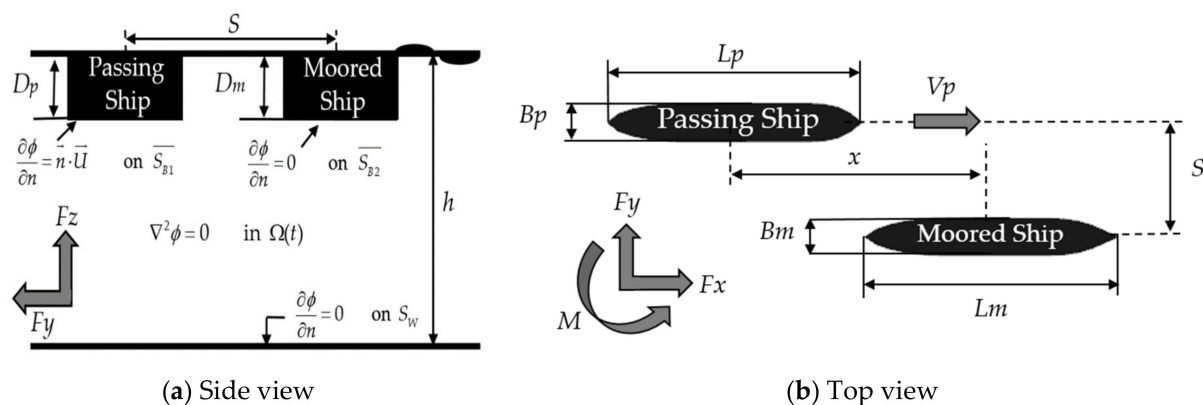


**Figure 1.** Linear boundary value problem and definition of the variables of the passing ship problem: (a) side view and (b) top view.  $V_p$ : passing ship speed,  $S$ : separation distance,  $L$ : length,  $B$ : breadth,  $D$ : draft,  $h$ : water depth.

The governing equation for the potential flow is the Laplace equation as shown in Equation (1), where  $\phi$  is the velocity potential defined in the fluid domain  $\Omega(t)$ . Equation (2) indicates the body boundary conditions on the wetted surface area ( $\overline{S_{B1}}, \overline{S_{B2}}$ ) of the ships, where  $\vec{U}$  is the velocity vector of the ship and  $\vec{n}$  is the unit normal vector. The fluid domain varies with time due to the moving boundary  $\overline{S_{B1}}(t)$  of the passing ship. If the moored ship is fixed ( $\vec{U} = 0$ ), then the right-hand side of Equation (2) becomes zero. Equation (3) represents the normal velocity boundary condition at the mean water level ( $z = 0$ ) and on the seabed ( $z = -h$ ). Previous studies confirmed that the suction effect, a primary factor of low-speed passing ships, can be calculated through the double-body model [18]. As this model neglects free-surface fluctuations, the time-dependent terms disappear in the boundary conditions. Therefore, the time integration method is not required, which reduces the total calculation time significantly. As a result, predicting real-time passing ship loads can be made possible using the double-body model [19].

Unlike the double-body model, the free-surface model applied Equations (4) and (5) as the free-surface boundary conditions instead of Equation (3). Here,  $\zeta$  is the wave elevation on the free surface, and  $g$  is the gravitational constant.

$$\frac{\partial \phi}{\partial t} = -g\zeta \quad \text{on } z = 0 \quad (4)$$

$$\frac{\partial \zeta}{\partial t} = \frac{\partial \phi}{\partial z} \quad \text{on } z = 0 \quad (5)$$

## 2.2. Numerical Method: Finite Element Method

In this study, a classical FEM was introduced to solve the Laplace equation in the fluid domain. The weak formulation of the Laplace equation was obtained by multiplying the test function  $\psi$  and applying the integration by parts, which results in Equation (6).

$$\iiint_{\Omega} \nabla \phi \cdot \nabla \psi dV - \iint_{\partial \Omega} \frac{\partial \phi}{\partial n} \psi dS = 0 \quad (6)$$

In the FEM, the fluid domain is discretized with a finite number of elements, and the velocity potential and wave elevation are approximated with 3D and 2D elements, respectively, as shown in Equations (7) and (8). In this study, the velocity potential was approximated using the linear summation of the product of the nodal velocity potential and the 3D basis function of eight-node hexahedral elements. The wave elevation was approximated using the linear summation of the product of the nodal wave elevation and the 2D basis function of the four-node quadrilateral elements.

$$\phi(x, y, z, t) = \sum_i \phi_i(t) N_i(x, y, z) \quad (7)$$

$$\zeta(x, y, t) = \sum_k \zeta_k(t) M_k(x, y) \quad (8)$$

By integrating Equation (6) with Equations (7) and (8), a linear algebraic equation can be derived. In the free-surface model, the wave elevation, as well as the velocity potential, is updated at each time step by applying the time integration of the free-surface boundary conditions. However, in the double-body model, only the velocity potentials are calculated, without any time integration of the free surface. In this study, the conjugate gradient method and the fourth-order Adams–Bashforth–Moulton method were used for matrix solving and the time integration on the free surface, respectively. The numerical method applied here can also be validated by solving a conventional ship resistance problem (Nam [12]).

The computation procedure for solving the passing ship problem is depicted in Figure 2. It can be divided into two parts according to the free-surface boundary conditions, i.e., the double-body and free-surface models. First, for the simulation, the program reads inputs of computation variables and ship geometry. The computation variables include the analysis domain, grid information, and simulation parameters. The ship geometry may be defined as  $x$ - and  $z$ -coordinate information for each section of the ship. Then, according to the horizontal position of the passing ship, the computational mesh is modified based on the re-mesh algorithm proposed by Nam [12]. In this study, the mesh generation technique was supplemented so that the local mesh is generated by extending it to the seabed or sidewall, which can be applied to the simulation case where the passing ship moves at a shallow water depth or has a low separation distance from the moored ship.

In the re-mesh algorithm, the mesh is divided into background, local and global meshes, as shown in Figure 3. First, the background mesh is generated for the entire computational domain, while local meshes are generated in a smaller area as body-fixed meshes containing the passing ship or moored ship hulls. As the simulation time progresses, the local mesh of the passing ship is moved according to the forward speed, whereas that of the moored ship is fixed at a specific location. Both local meshes are placed at their corresponding locations on the background mesh. Subsequently, the background meshes, which overlap with local meshes, are extracted and replaced with local meshes. Finally, by connecting their interfaces, an earth-fixed global mesh is generated. For a more generalized connection process, a background mesh is generated based on a rectangular 3D rectilinear grid, and local meshes are generated based on a rectangular 3D curvilinear grid considering that the passing ship moves parallel to the moored ship. In this way, both mesh interfaces

become a 2D rectilinear grid, and the global mesh based on the 3D rectilinear grid is completed through a straightforward connecting process.

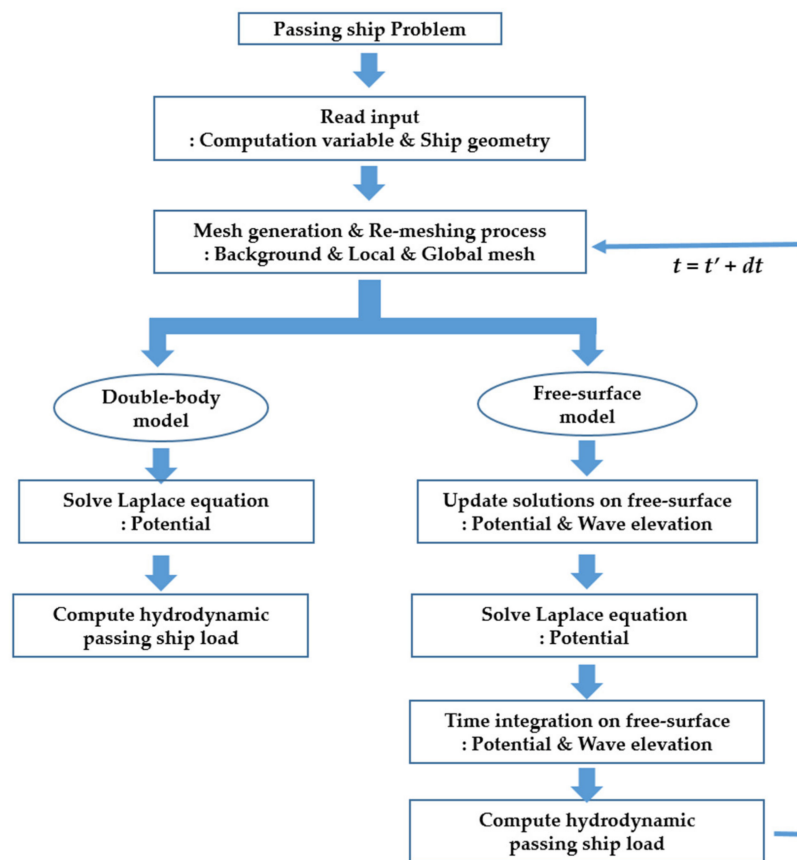


Figure 2. Computation procedure for the passing ship problem.

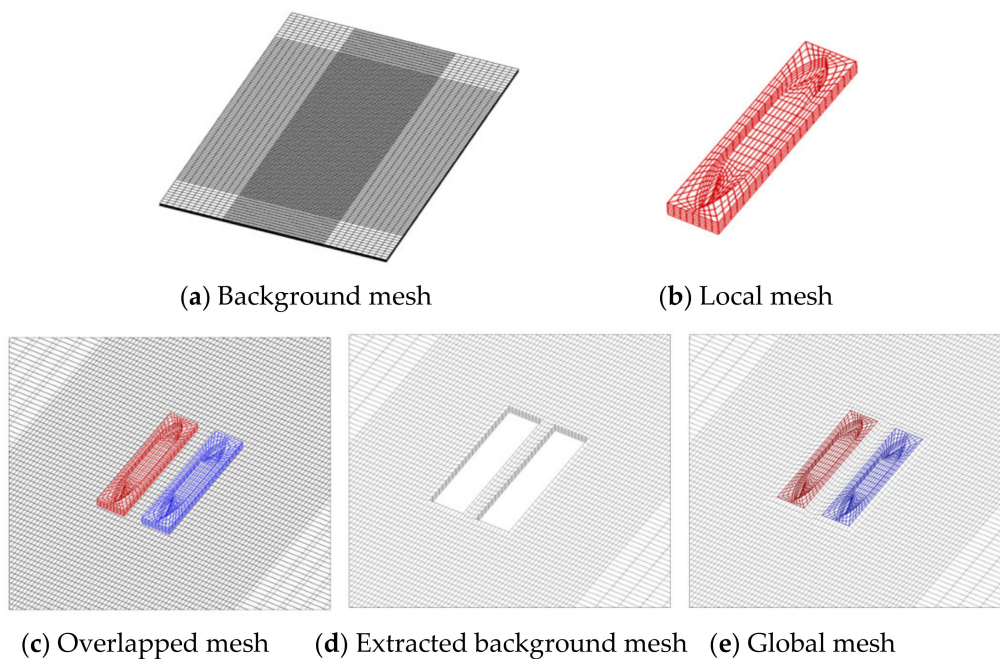
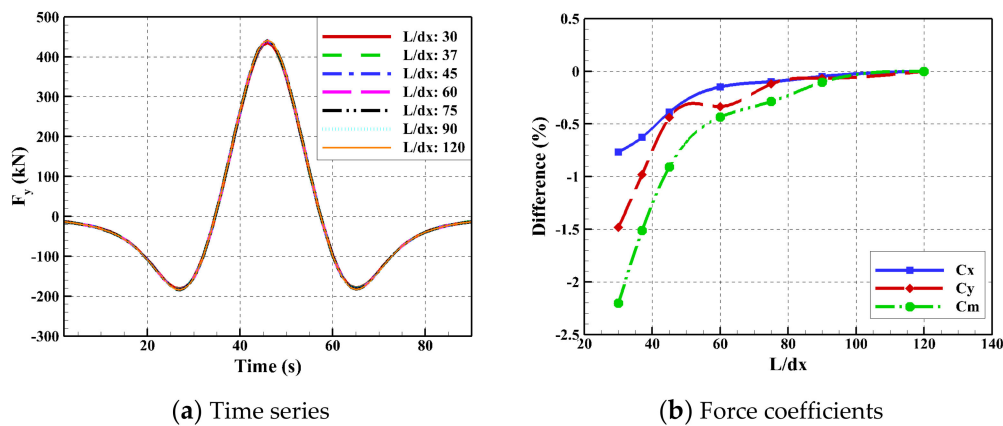


Figure 3. Re-mesh algorithm for the generation of a global mesh: (a) background mesh, (b) local mesh, (c) overlapped mesh, (d) Extracted background mesh, (e) Global mesh.

### 2.3. Convergence Study

Numerical studies were conducted on mesh convergence to determine the appropriate mesh size for accurate computations of the hydrodynamic forces due to the passing ship. Here, the mesh size was represented by the number of elements per mean ship length ( $L/dx$ ), which varies from 30 to 120. Figure 4a shows the convergence test results in terms of the time histories of sway force according to different mesh sizes. It is evident that all the computational results were almost the same regardless of the mesh size, which indicates the convergence of numerical solutions. For a more precise comparison, the positive peak values of the surge and sway forces and yaw moment can be compared, as shown in Figure 4b. The computational results were represented by the difference in each load compared to that of the finest mesh ( $L/dx = 120$ ). It is confirmed that the largest difference was less than 2.5% of the yawing moment for the coarsest grid. Thus, all hydrodynamic forces converged quickly as the mesh size decreased. Hereafter, numerical computations were performed by applying  $L/dx = 60$ , in which all load coefficients converge within an error of less than 0.5%.



**Figure 4.** Convergence test results of the passing ship forces in terms of the (a) time series and (b) force coefficients.

### 2.4. Simulation Description

The numerical simulations were performed by varying the Froude number, the separation distance ( $S$ ) between the passing and moored ships, and the water depth ( $h$ ), as shown in Figure 1. Regarding the Froude numbers, the length-based Froude number is defined as  $F_L = V_p / \sqrt{gL}$ , while the depth-based Froude number defined as  $F_h = V_p / \sqrt{gh}$ . The computational results were validated by comparison with the data from Kriebel's model tests [5]. Generic Series 60 hull forms were used as the passing and moored ship hulls (Figure 5, [20]), and the variable ranges in this study, as listed in Table 1, were the same as those of Kriebel's model test [5]. Further analysis was also conducted by varying the moored ship size ( $L_m \times B_m \times D_m$ ) to examine its effect. In each part of the analysis, the target variable was changed within a given range (Table 2), whereas the other variables were fixed using the representative values summarized in Table 1.

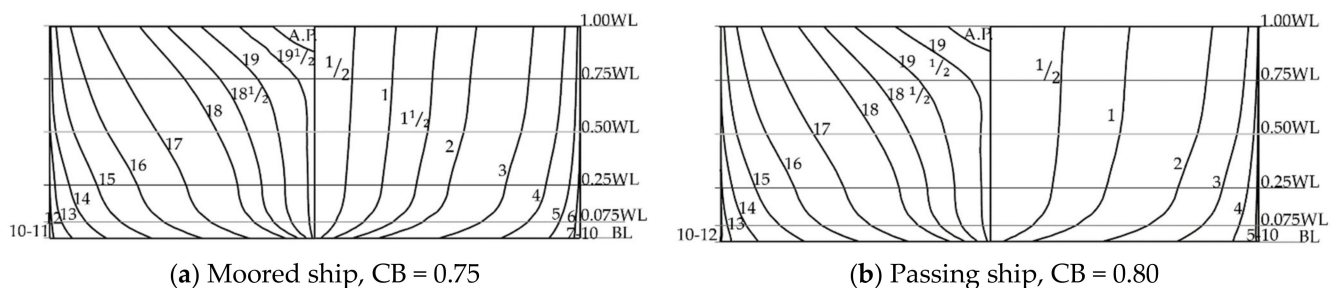


**Figure 5.** Series 60 hull lines for (a) moored ship with  $C_B = 0.75$  and (b) passing ship with  $C_B = 0.80$ .

**Table 1.** Calculation variable ranges.  $F_L$ :  $V_p/\sqrt{gL}$ ,  $V_p$ : passing ship speed,  $S$ : separation distance,  $L$ : length,  $B$ : breadth,  $D$ : draft,  $h$ : water depth.

Variable	$F_L$	$S/L$	$h/D$	Moored Ship
Representative	0.142	0.4	1.324	Series 60
Number of cases	6	5	6	2
Range	0.063–0.163	0.3–1.0	1.108–3.919	Series 60/Barge

**Table 2.** Calculation variable list for (a) Froude number, (b) separation distance, and (c) water depth.  $F_L$ :  $V_p/\sqrt{gL}$ ,  $F_h$ :  $V_p/\sqrt{gh}$ ,  $V_p$ : passing ship speed,  $S$ : separation distance,  $L$ : length,  $B$ : breadth,  $D$ : draft,  $h$ : water depth.

(a) Froude Number		
No.	$F_L$	$F_h$
1	0.063	0.222
2	0.080	0.281
3	0.104	0.365
4	0.124	0.435
5	0.142	0.498
6	0.165	0.578
(b) Separation Distance		
No.	$S/L$	$S/B$
1	0.30	2.02
2	0.40	2.70
3	0.60	4.05
4	0.80	5.39
5	1.00	6.74
(c) Water Depth		
No.	$h/D$	$D/h$
1	1.108	0.902
2	1.216	0.822
3	1.324	0.755
4	1.486	0.673
5	2.270	0.440
6	3.919	0.255

### 3. Simulation Results and Discussions

#### 3.1. Double-Body vs. Free-Surface Models

First, the hydrodynamic forces acting on a moored ship were calculated when a passing ship travels far from the moored ship and moves parallel to it. In this case, the distance between the moored and passing ships initially becomes closer as time passes. Then, the passing ship moves next to the moored ship, where the hydrodynamic interaction becomes most significant. Finally, the passing ship moves away. The horizontal hydrodynamic forces and moment acting on the moored ship due to the passing ship are shown in Figure 6. Here, the  $x$ -axis represents the non-dimensional horizontal distance, which is the ratio of the horizontal distance between two ships to the mean ship length. The  $y$ -axis represents the non-dimensional force and moment coefficients defined by Equation (9). In these plots, the computational results of the double-body (DB) and free-surface (FS) models are directly compared and the peak values from Kriebel's model test [5] are plotted together as dash-dot horizontal lines. As shown in Figure 6, the two numerical results show similar trends, including the positions at which the force peaked. However, it can be observed that the amplitudes of the surge, sway forces, and yaw moment of the FS model were slightly larger than those of the DB model. In addition, small wave-frequency force components are also observed due to the small waves caused by the passing ship in the numerical

simulation of the FS model. When comparing the experimental data, the results of the FS model are relatively closer to the experimental data than that of the DB model.

$$C_x = \frac{F_x}{0.5\rho DLV^2}, C_y = \frac{F_y}{0.5\rho DLV^2}, C_m = \frac{M}{0.5\rho DL^2V^2} \quad (9)$$

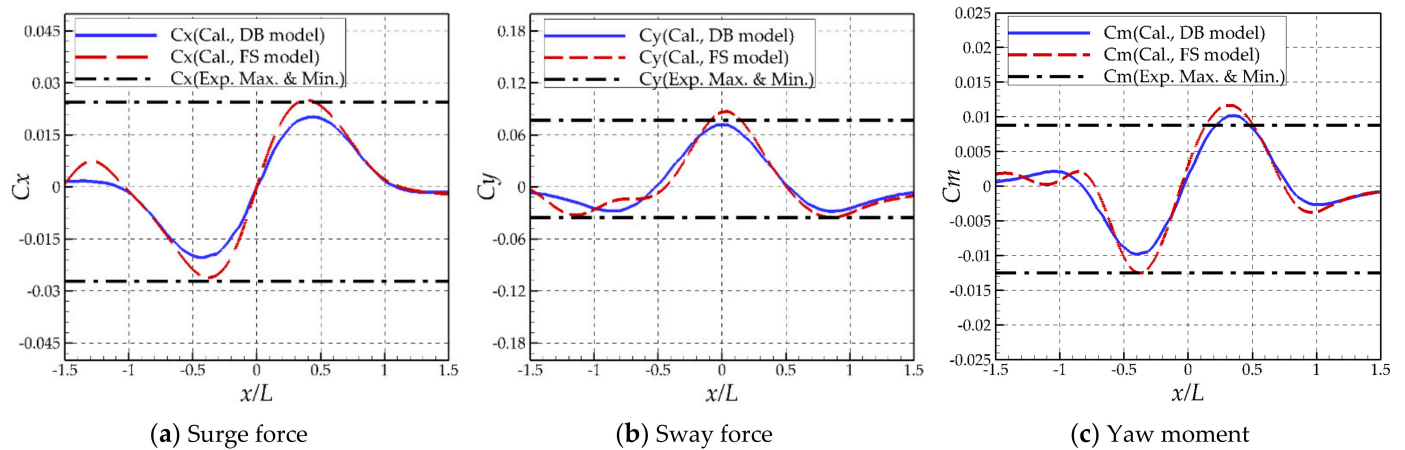


**Figure 6.** Comparison of the time series of horizontal hydrodynamic forces and moment between two numerical results and experiment: (a) surge force, (b) sway force, (c) yaw moment ( $Fn = 0.142$ ,  $S/L = 0.4$ ,  $h/D = 1.324$ ).

The speed of the passing ship is known to be the most important factor in the hydrodynamic problem of a passing ship [3,5]. In this study, numerical simulations were conducted according to various Froude numbers, as listed in Table 2. The present computational results were compared with the experimental data in Figure 7. The  $x$ -axis represents the Froude number, whereas the  $y$ -axis shows the peak values of the passing ship forces and moment. As expected, the hydrodynamic forces and moment significantly increase with the speed of the passing ship. Regarding the surge and sway forces, it can be seen that the computational results of the FS model are closer to the model test data than those of the DB model. In the case of the DB model, the hydrodynamic forces increase in proportion to the square of the passing ship speed. However, the model test and the FS model show that the passing ship forces increase more than the square of the passing ship speed due to the free-surface effect. Kriebel et al. [21] also reported that, if the depth-based Froude number is greater than 1.0 and the passing ship speed exceeds the wave celerity, the ship wave can be generated excessively, causing a significant free-surface effect. In addition, the free-surface effect also becomes important when the length-based Froude number is 0.4, and the transverse wavelength equals the ship length. As our simulation results indicate, the DB model could estimate the passing ship loads with similar accuracy to the FS model until the length-based Froude number became 0.12. However, if the passing ship speed exceeded this speed range, the results of the FS model and model test resulted in a difference of more than 10% from those of the DB model. When looking at the yaw moment results, the increasing tendency of the yawing moment from two present numerical calculations was similar to that of the model test even though some differences were observed.

For a more detailed analysis, the potential and pressure fields on the free surface were computed using the DB model, as shown in Figure 8. In each column,  $x/L$  of the passing ship ( $x$ : defined in Figure 1) corresponds to  $-0.5$ ,  $0$ , and  $+0.5$ , hereinafter referred to as P1, P2, and P3, respectively. When compared with the time series of the surge force in Figure 6a, the surge force showed negative and positive peak values at P1 and P3, respectively. At these locations, the center of the moored ship is close to the positive and negative pressure field regions. When the passing ship arrives at P2, the midships of the passing and moored ships are abreast, and it can be observed that an almost symmetrical pressure field also forms around the moored ship. As a result, the surge force acting on the moored ship

becomes nearly zero at P2. Therefore, the time series of the surge force shows a sine-wave shape symmetrical at  $x/L = 0$ , as shown in Figure 6a.

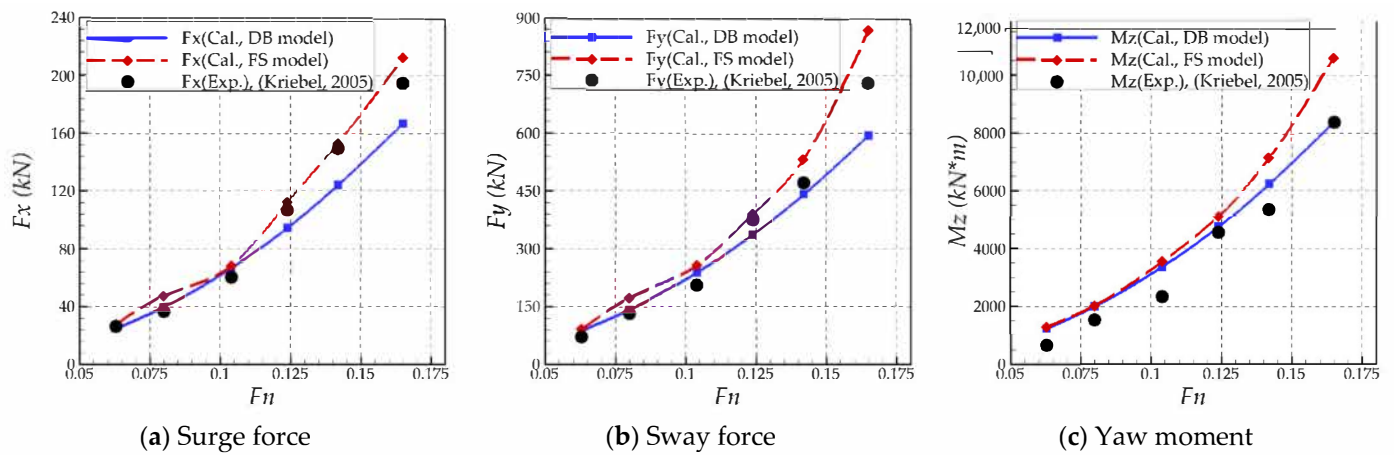


**Figure 7.** Effect of passing ship speed on the hydrodynamic forces and moment acting on the moored ship: (a) surge force, (b) sway force, (c) yaw moment ( $S/L = 0.4$ ,  $h/D = 1.324$ ).

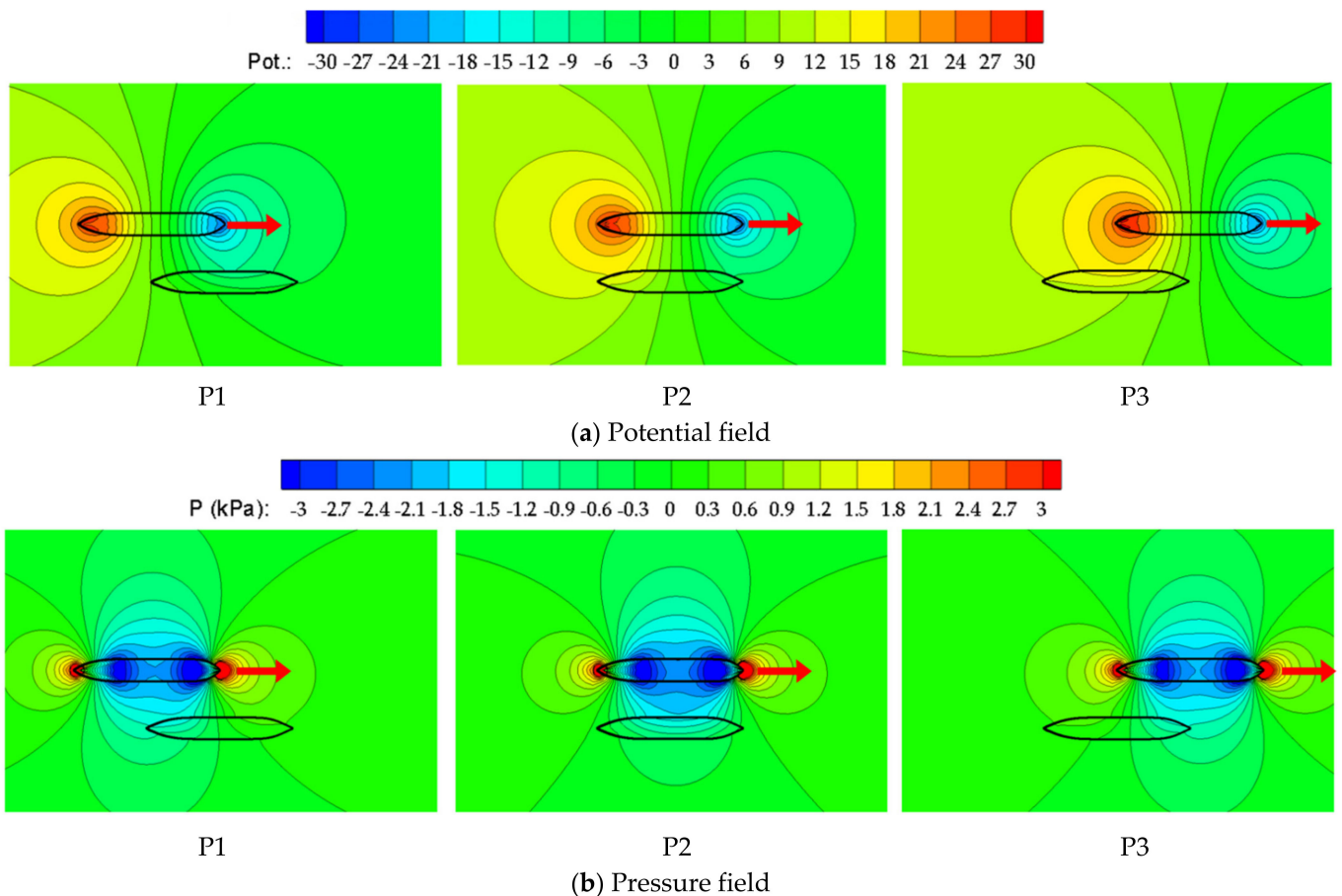


**Figure 8.** Potential and pressure fields of the double-body model with  $x/L$  of  $-0.5$ ,  $0$ , and  $+0.5$ : (a) potential field, (b) pressure field ( $F_n = 0.142$ ,  $S/L = 0.4$ ,  $h/D = 1.324$ ).

Regarding the sway force, the maximum positive value is found at P2, where the moored ship is located at the center of the negative pressure field. The positive sign of the sway force indicates that the moored ship is pulled toward the passing ship. When

$x/L$  is  $-0.75$  and  $+0.75$ , maximum negative sway forces are exerted on the moored ship in a direction away from the passing ship. At these positions, the moored vessel is directly affected by the positive pressure fields around the bow or stern of the passing ship, which results in a strong repulsive force between the passing and moored ships. The time series of sway force shows the shape of the cosine wave to be symmetrical about the  $y$ -axis, and the positive peak value is approximately twice the negative peak value. This is because, as shown in Figure 8b, when looking at the pressure field that affects the moored ship, the negative pressure field near the middle of the passing ship is almost twice as strong as the positive pressure field around the bow or stern. The yaw moment also shows a sine-wave shape, symmetric at  $x/L = 0$ . The negative peak, zero value, and positive peak of the yaw moment were observed at P1, P2, and P3, respectively. It can be seen that the yaw moment acting on the moored ship is determined by the lateral force and its application point.

The potential, pressure, and wave elevation fields obtained by the FS model are shown in Figure 9. The potential and pressure show a similar spatial distribution to the results of the DB model. However, the magnitude of the pressure in the FS model is slightly greater. In addition, a slightly asymmetric pressure field can be found around the bow and stern sections of the moored ship. The wave elevation field of the FS model also shows a similar spatial distribution to that of the pressure field. For a more rigorous comparison of the amplitude of the pressure for both models, the cross-sectional pressure fields at  $x/L = 0$  are calculated in Figure 10. It can be seen that a high pressure field forms around the moored ship because of the wave elevation, which results in the higher forces of the passing ship.

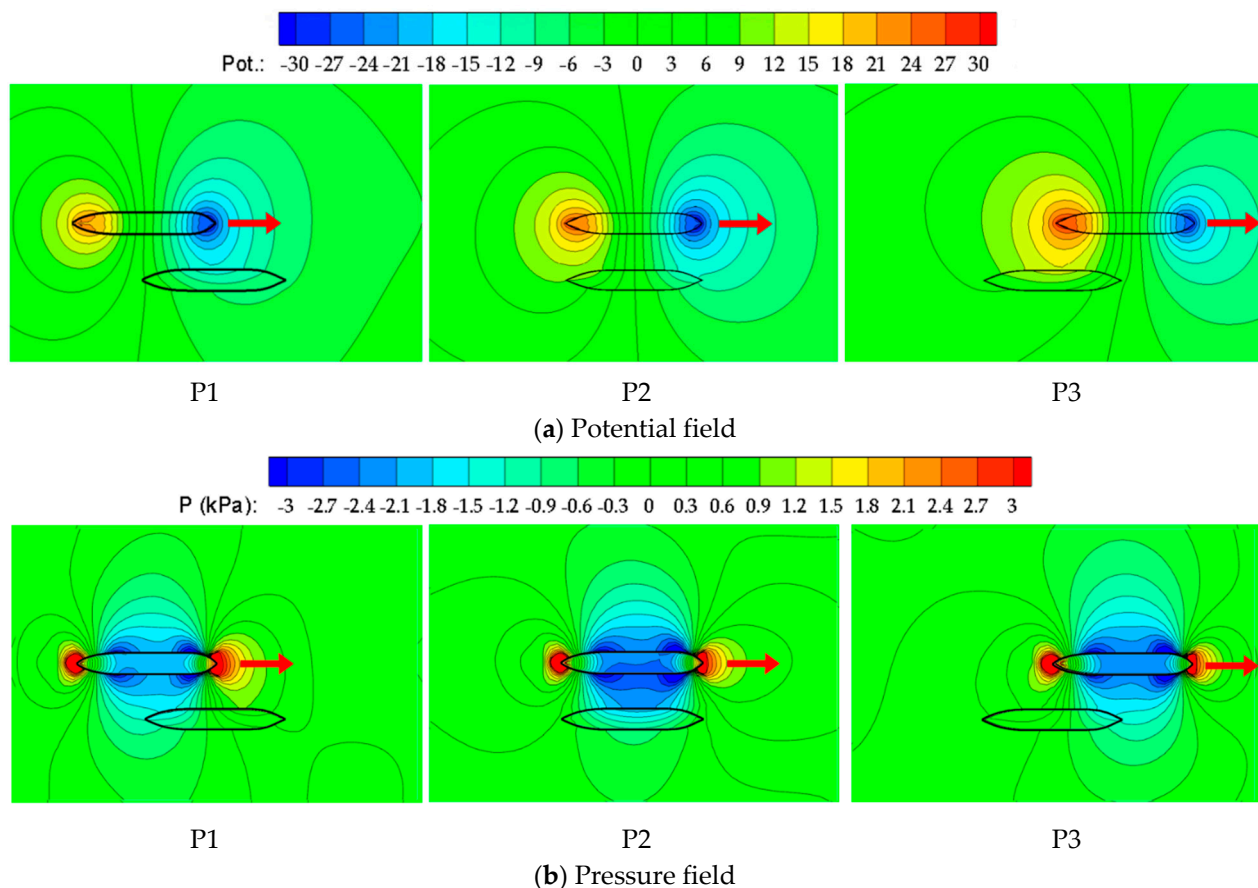
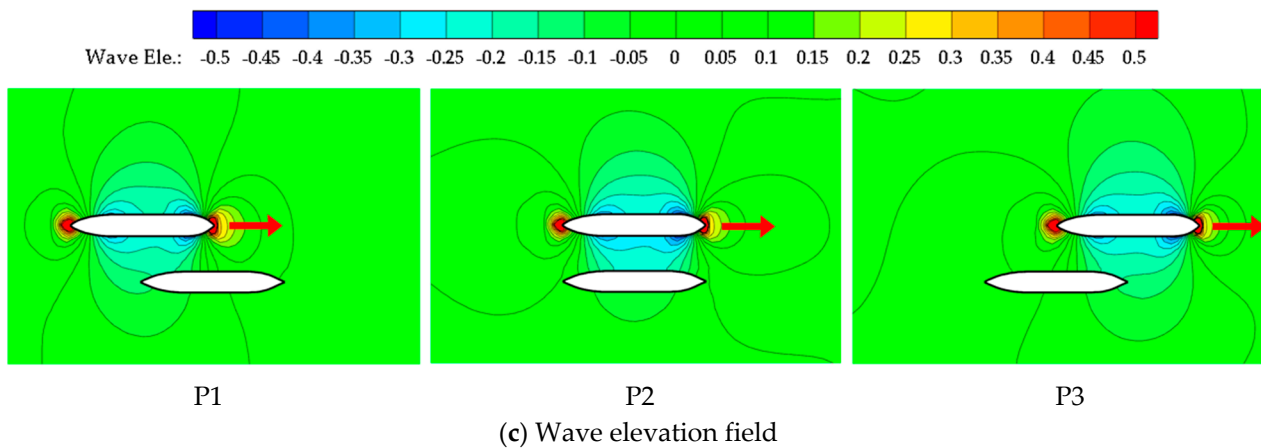
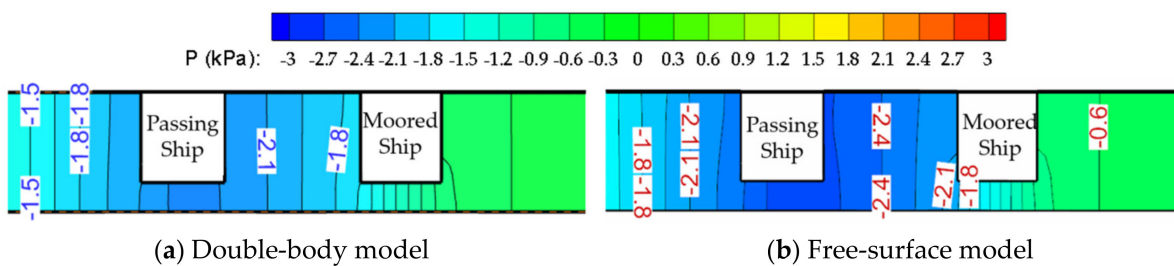


Figure 9. Cont.



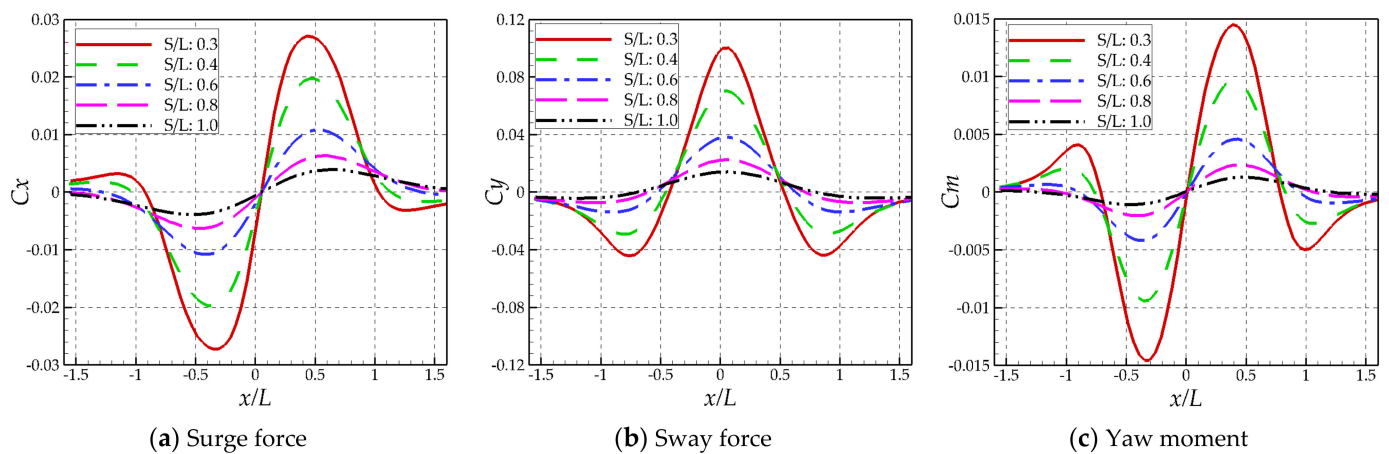
**Figure 9.** Potential, pressure, and wave elevation fields of the free-surface model with  $x/L$  of  $-0.5$ ,  $0$ , and  $+0.5$ : (a) potential field, (b) pressure field, (c) wave elevation field ( $Fn = 0.142$ ,  $S/L = 0.4$ ,  $h/D = 1.324$ ).



**Figure 10.** Cross-sectional pressure fields of the (a) double-body and (b) free-surface models with  $x/L$  of  $0$  ( $Fn = 0.142$ ,  $S/L = 0.4$ ,  $h/D = 1.324$ ).

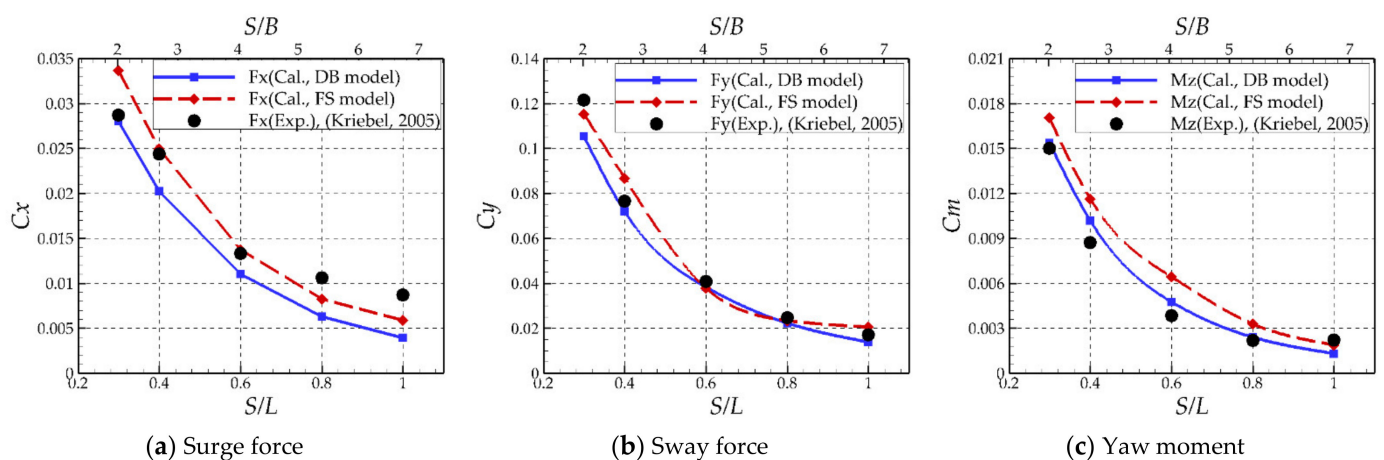
### 3.2. Effects of Separation Distance and Water Depth

For analyzing the effect of separation distance, numerical simulations were performed under various separation distances, which were defined as the horizontal distances between the centerlines of the passing ship and moored ship. The range of the ratio of the separation distance to ship length ( $S/L$ ) is  $0.3$ – $1.0$ . The minimum separation distance ratio  $S/L = 0.3$  corresponds to the ship length-to-breadth ratio ( $S/B$ ) of  $2.0$ , which means that the distance between the two ships' sidewalls is equal to the ship breadth. In the present analyses, the Froude number was fixed at  $0.142$ , and the depth-to-draft ratio at  $1.324$ . Figure 11 shows the computational results of the DB model under various separation distance conditions. Here, the time series of the hydrodynamic forces and moment by the passing ship are directly compared. As the separation distance increases, the amplitudes of the passing ship loads significantly reduce, and the phase angles also slightly change. The peak sway forces are observed at the position where  $x/L$  is  $0$ , regardless of the separation distance. However, the positions where the maximum surge forces or the maximum yaw moments are observed are far from the intersection position. Here,  $x/L$  changes from  $0.3$  to  $0.5$  with an increase of separation distance. This is because the maximum surge forces occur when the moored ship is located at the boundary between the positive and negative pressure, as shown in Figure 9b. As the separation distance increases, the boundary also moves farther from the intersection position.



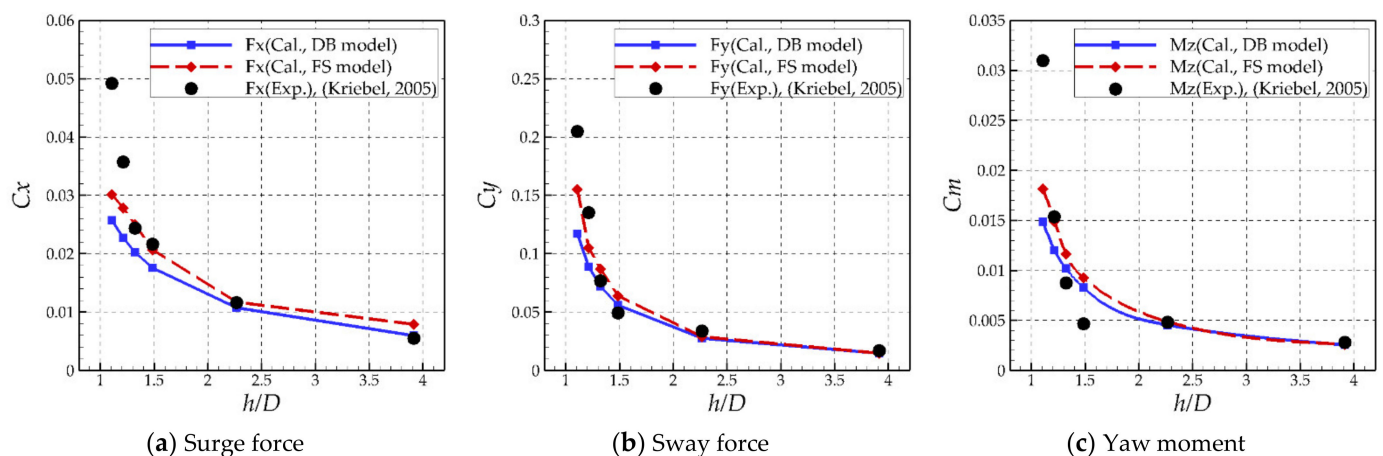
**Figure 11.** Comparison of the time series of passing ship forces and moment with various separation distances: (a) surge force, (b) sway force, (c) yaw moment ( $Fn = 0.142$ ,  $h/D = 1.324$ ).

Figure 12 shows the effect of the separation distance on the passing ship forces by comparing the results of the computations and experiments. Here, the  $x$ -axis shows two types of non-dimensional separation distance ratios,  $S/L$  and  $S/B$ . The  $y$ -axis denotes the non-dimensional force and moment coefficients divided by the square of the passing ship speed, as given in Equation (9). In general, as the separation distance decreases, the passing ship forces can be expected to increase. It can be clearly seen that the forces and moment sharply increase when the separation distance decreases, especially to less than four times the breadth. As shown in Figure 9b, when the two ships get closer, a strong hydrodynamic pressure field develops between them. Overall, the experimental result and numerical simulations showed similar trends for the passing ship forces and moment according to the various separation distances. For the surge and sway force coefficients, the FS model results showed slightly higher load coefficients than those of the DB model, and the model test results were closer to the former. For all separation distances, the sway forces were about four times larger than the surge force. Regarding the yaw moment coefficient ( $C_m$ ), the model test data were slightly lower than the computational results. However, the increasing tendency of the yawing moment in both the model test data and numerical results was similar. It should be noted that the differences in computational results of the DB and FS models were still observed to be approximately 10–20% with respect to the values of the DB model.



**Figure 12.** Effect of separation distance on the hydrodynamic forces and moment acting on the moored ship: (a) surge force, (b) sway force, (c) yaw moment ( $Fn = 0.142$ ,  $h/D = 1.324$ ).

As the passing ship sometimes needs to pass a location in shallow waterways or coasts on a given route, the water depth is also a critical simulation parameter for the passing ship problem. Additional numerical simulations were performed to study its effect on the passing ship loads. Here, the depth-to-draft ratio ( $h/D$ ) was varied from 1.108 to 3.919, and the other parameters were fixed at their representative values with a length-based Froude number of 0.142 and  $S/L$  of 0.4. The lowest water depth ratio, i.e., 1.108, represents a distance between the bottom of the ship and the seabed of only 10% of the ship's draft. Numerical computations were performed by applying both DB and FS models, and the load coefficients were compared with the model test results, as shown in Figure 13. It can be seen that the passing ship forces increase as the water depth decreases. In particular, as the water depth gets shallower,  $h/D < 1.5$ , the load increases exponentially due to the seabed effect. Under the deep water-depth conditions of  $h/D = 1.5$  or more, the loads for the computation and model test results were similar, with the effect of the water depth on the ship-generated wave no longer being prominent. However, at shallow depths with  $h/D < 1.5$ , the computation and model test results showed significant discrepancies (in the order of the double-body model, free-surface model, and model test results). At shallower depths where  $h/D < 1.2$ , the difference between the results of the FS model and the experiment significantly increased because, as the water depth decreases, nonlinear effects, such as those of viscosity and nonlinear waves, increase. Calculations for deeper water depth conditions with  $h/D > 4$  were also performed as a representative of a water depth at which the seabed effect would not affect the passing ship load anymore. As a result, the variation of the passing ship load according to the increase of the water depth was less than 5% when  $h/D > 10$ . This result means that the pressure field near the water surface is formed without being affected by the seabed effect, and therefore the water-depth effect should be considered if the water depth is shallower than ten times the ship's draft.



**Figure 13.** Effect of depth–draft ratio on the hydrodynamic forces and moment acting on the moored ship: (a) surge force, (b) sway force, (c) yaw moment ( $Fn = 0.142$ ,  $S/L = 0.4$ ).

### 3.3. Effect of Ship Size

In this section, the size effect on the passing ship problem is discussed. The passing ship problem is a phenomenon caused by the hydrodynamic interaction between passing and moored ships, so their relative sizes are a critical factor for the passing ship problem. The passing ship was selected as a Series 60 hull with a block coefficient of 0.80, while the moored ship was considered as a rectangular barge so that the length, breadth, and draft could be easily varied (Figure 14 and Table 3). For analyzing the size effect, the sizes of the barge were varied in each direction independently. Numerical computations were performed by applying the DB model. Figure 15 compares the time series of the hydrodynamic forces and moment acting on the Series 60 and barge. The pressure fields on the water surface are also compared in Figure 16. It can be observed that  $C_y$  increases

slightly, and  $C_m$  increases significantly owing to the shape of the moored ship, although  $C_x$  remains constant. The reasons for the increases in  $C_y$  and  $C_m$  were due to increases in the surface area at the bow and stern of the barge and in the pressure difference between the port and starboard sections of the barge. The peak loads were observed at similar horizontal distances for the results of both the Series 60 and barge.

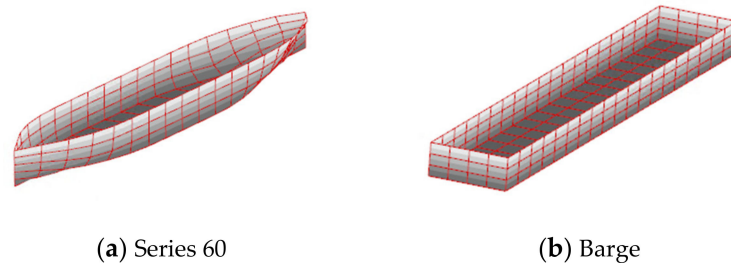


Figure 14. Comparison of hull forms between (a) Series 60 ship and (b) barge.

Table 3. Comparison of main dimensions for the passing and moored ships.

	Passing Ship	Moored Ship 1	Moored Ship 2
Hull	Series 60, $C_B = 0.80$	Series 60, $C_B = 0.75$	Barge
Length(m)	100	100	100
Breadth(m)	15.33	14.83	14.83
Draft(m)	6.17	6.17	6.17

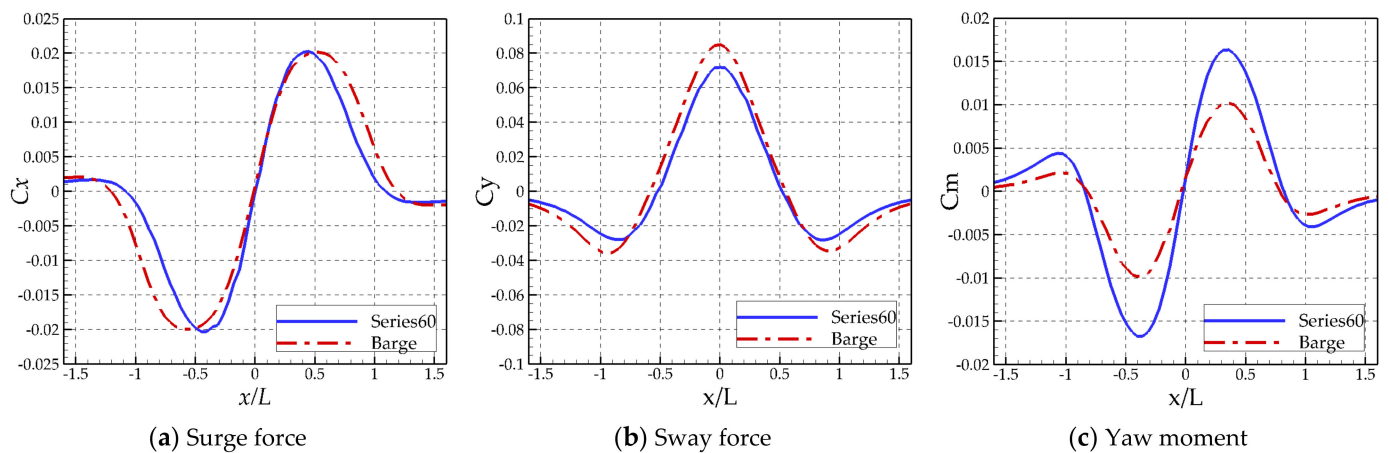


Figure 15. Comparison of the time series of passing ship forces and moment acting on the Series 60 ship and the barge: (a) surge force, (b) sway force, (c) yaw moment ( $Fn = 0.142$ ,  $S/L = 0.4$ ,  $h/D = 1.324$ ).

For the analysis of the size effect, the breadth ratio ( $B/B_0$ ) was varied within 75–100%, and the length ratio ( $L/L_0$ ) within 80–120%. Figure 17a shows the changes in hydrodynamic forces according to variations of the barge breadth. The  $x$ -axis represents the change in the breadth ratio as a percentage. The  $y$ -axis represents the ratio of the force or moment coefficients acting on the re-sized barge compared to the original Series 60 with a block coefficient of 0.75. It can be seen that all the forces and moment linearly increase as the breadth of the moored ship increases. Specifically, as the ship breadth increases by 10%, the surge and sway forces and yaw moment coefficients also increase by approximately 10%.

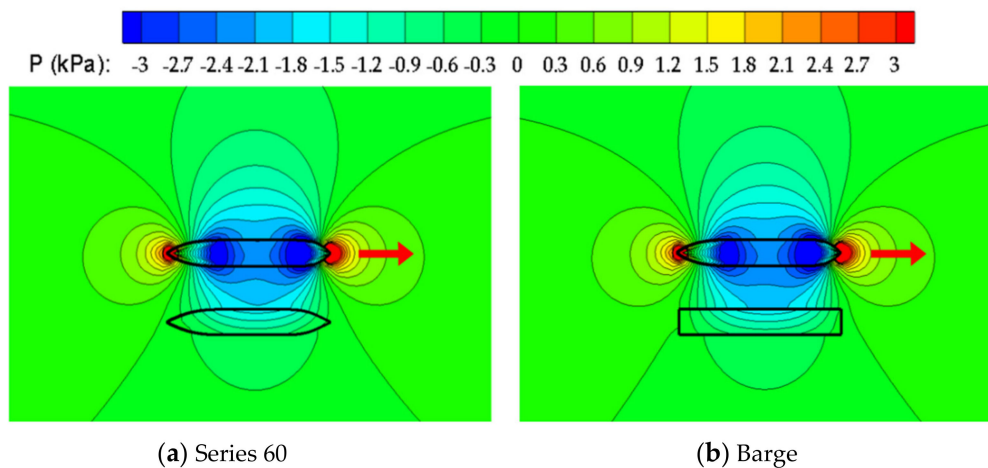


Figure 16. Pressure field around the moored (a) Series 60 ship and (b) barge ( $x/L = 0$ ,  $Fn = 0.142$ ,  $S/L = 0.4$ ,  $h/D = 1.324$ ).

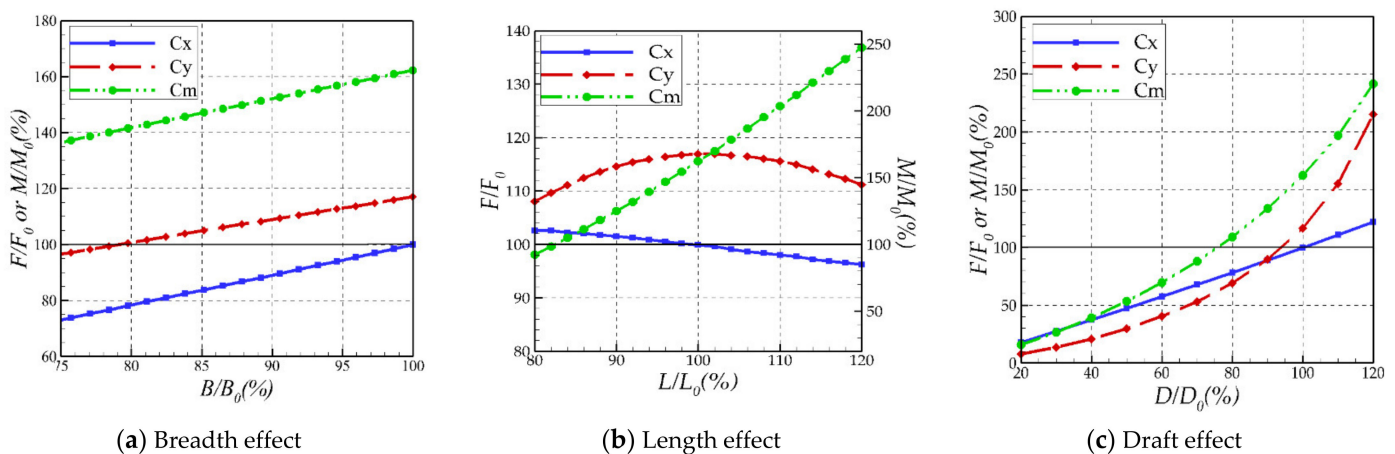


Figure 17. Differences in the load coefficients according to (a) breadth, (b) length and (c) draft variations ( $Fn = 0.142$ ,  $S/L = 0.4$ ,  $h/D = 1.324$ ).

According to the change in length of the barge, the load coefficients for the surge and sway forces and yaw moment were also calculated and compared to the basic loads acting on the original Series 60, as shown in Figure 17b. As the moored ship length increases, the surge force decreases linearly; however, the yaw moment increases linearly. As the moored ship's length increases, the bow or stern section of the moored ship move to the low-pressure field region, which results in the decrease of the surge force. However, the resultant yaw moment increases because the surface area at the port side on which the lateral force is exerted increases. It can be observed that the maximum sway force occurs when the passing and moored ships have the same length. This is because, if the moored ship length is lower than the passing ship length, the lateral area on which the positive sway force is exerted also reduces. On the contrary, if the length of the moored ship is greater than that of the passing ship, then the area under the negative pressure field remains the same, but the area of the positive pressure field around the bow and stern sections increases, as shown in Figure 16b. As a result, as the ship length ratio ( $L/L_0$ ) increases from 90% to 100%, the surge force is reduced by 2%, sway force increases by 3%, and the yaw moment increases by 15%.

The computations were also conducted by changing the draft ratio ( $D/D_0$ ) from 10% to 120%, as shown in Figure 17c. It can be seen that the surge force linearly increases due to the linear increase in the area at the bow and stern sections from which the pressure fields are formed; however, the sway force and yaw moment exponentially increase with

$D/h$ . As the draft increases, the exponential indices of the sway force and yaw moment increase from 2 and 1.4 to 3 and 2, respectively. Compared to the analysis of the breadth and length change, the passing ship load increases more rapidly when the draft varies. This is because the seabed effect is added to the effect of the increase in the surface area due to the reduction in the gap between the bottom of the ship and the seabed under the fixed water-depth condition.

#### 4. Conclusions

In this study, the hydrodynamic forces acting on a moored ship caused by a passing ship were analyzed through a series of FEM-based numerical computations. The results are summarized as follows.

- The hydrodynamic forces and moment acting on the moored ship increase significantly as the speed of the passing ship increases. In particular, the passing ship load increases in proportion to the square of the passing ship speed under low Froude numbers less than 0.12, for which both the DB and FS models can accurately predict the passing ship loads. However, when the Froude number exceeds this limit, the passing ship load increases at a rate faster than the square of the passing ship speed, mainly due to the free-surface effect. Under this condition, it was found that the numerical results based on the FS model were closer to the model test data than those based on the DB model.
- The passing ship loads increase gradually with decreasing separation distance between the passing and moored ships. From the present numerical computations, it can be observed that the passing ship loads sharply increase when the separation distance ratio ( $S/B$ ) becomes less than 4. Under low-speed conditions, the present numerical methods could predict the peak values of the passing ship loads with an error less than 10%, regardless of the separation distance.
- As the water depth decreases, the passing ship load also increases. Especially under shallow water-depth conditions where the depth ratio ( $h/D$ )  $< 1.2$ , it could be clearly observed that the passing ship loads significantly increased.
- The relative sizes of the moored and passing ships are a critical factor in the passing ship loads due to changing pressure fields formed around the moored ship. All the forces and moment increase linearly with increasing moored ship breadth. Furthermore, with an increase in the moored ship length, the surge force linearly decreases, and the yaw moment linearly increases. Compared to the changes in the breadth and length, passing ship loads are more sensitive to the change of the ship draft.
- In the future, new validation data from model tests are required for a close examination of the free-surface effect in the passing ship problem. In addition, numerical studies on various ships should be performed by applying the developed numerical methods.

**Author Contributions:** Conceptualization, J.-Y.P. and B.W.N. and Y.K.; methodology, J.-Y.P. and B.W.N. and Y.K.; validation, J.-Y.P.; writing-original draft preparation, J.-Y.P.; writing-review and editing, B.W.N. and Y.K.; supervision, B.W.N. and Y.K. All authors have read and agreed to the published version of the manuscript.

**Funding:** This research was supported by Korea Research Institute of Ships and Ocean engineering, project number PES3980.

**Institutional Review Board Statement:** Not applicable.

**Informed Consent Statement:** Not applicable.

**Data Availability Statement:** Not applicable.

**Acknowledgments:** This research was supported by a grant from the Endowment Project “Development of WECAN for the Establishment of Integrated Performance and Structural Safety Analytical Tools of Wave Energy Converter” funded by the Korea Research Institute of Ships and Ocean engineering (PES3980).

**Conflicts of Interest:** The authors declare no conflict of interest.

## References

1. National Transportation Safety Board (NTSB). *Fire and Explosion Aboard the U.S. Tankship Jupiter*; U.S. Department of Transportation: Bay City, MI, USA, 1990.
2. Remery, G.F.M. Mooring forces induced by passing ships. In Proceedings of the Offshore Technology Conference, Dallas, TX, USA, 6–8 May 1974.
3. Muga, B.; Fang, S. Passing Ship Effects—From Theory and Experiment. In Proceedings of the Offshore Technology Conference, Houston, TX, USA, 5–8 May 1975.
4. Vantorre, M.; Verzhbitskaya, E.; Laforce, E. Model test based formulations of ship-ship interaction forces. *Ship Tech. Res.* **2002**, *49*, 124–141.
5. Kriebel, D. *Mooring Loads due to Parallel Passing Ships*; Technical Report; TR-6056-OCN; Naval Facilities Engineering Service Center: Port Hueneme, CA, USA, 2005.
6. Flory, J.F. The Effect of Passing Ships on Moored Ships. In Proceedings of the Prevention First 2002 Symposium, California State Lands Commission, Long Beach, CA, USA, 10–22 September 2002.
7. Seelig, W.N. *Passing Ship Effects on Moored Ships*; Technical Report; TR-6027-OCN; Naval Facilities Engineering Service Center: Port Hueneme, CA, USA, 2001.
8. Swiegers, P.B. Calculation of the Forces on a Moored Ship due to a Passing Container Ship. Ph.D. Thesis, Stellenbosch University, Stellenbosch, South Africa, 2011.
9. Wang, S. Dynamic effects of ship passage on moored vessels. *J. Waterw. Harb. Coast. Div. Am. Soc. Civ. Eng.* **1975**, *101*, 247–258.
10. Pinkster, J.A. The influence of a free surface of passing ship effects. *Int. Shipbuild. Progr.* **2004**, *51*, 313–338.
11. Van der Molen, W.; Rossouw, M.; Phelp, D.; Tulsi, K.; Terblanche, L. Innovative technologies to accurately model waves and moored ship motions. In Proceedings of the Science Real and Relevant Conference, Stellenbosch, South Africa, 30 August–1 September 2010.
12. Nam, B.W.; Park, J.Y. Numerical simulation for a passing ship and a moored barge alongside quay. *Int. J. Nav. Archit. Ocean Eng.* **2018**, *10*, 566–582. [[CrossRef](#)]
13. Park, J.Y.; Nam, B.W.; Kim, Y.H. Prediction of hydrodynamic forces on passing ships. In Proceedings of the International Workshop on Water Waves and Floating Bodies (IWWWFB), Virtual Workshop, 24–27 August 2020.
14. Huang, E.T.; Chen, H.C. Influences of ship specifics on passing ship effects. In Proceedings of the Sixteenth International Offshore and Polar Engineering Conference, Lisbon, Portugal, 1–6 July 2007.
15. Wang, H.Z.; Zou, Z.J. Numerical study on hydrodynamic interaction between a berthed ship and a ship passing through a lock. *Ocean. Eng.* **2014**, *88*, 409–425. [[CrossRef](#)]
16. Korsmeyer, F.T.; Lee, C.H.; Newman, J.N. Computation of Ship Interaction Forces in Restricted Waters. *J. Ship Res.* **1993**, *37*, 298–306. [[CrossRef](#)]
17. Pinkster, J.A.; Ruijter, M.N. The Influence of Passing Ships on Ships Moored in Restricted Waters. In Proceedings of the Offshore Technology Conference, Houston, TX, USA, 3–6 May 2004.
18. Pinkster, J.A. *Suction, Seiche and Wash Effects of Passing Ships in Ports*; PMH B.V.: Rotterdam, The Netherlands, 2009.
19. Pinkster, J.A. Progress on Real-Time Prediction of Ship-Ship-Shore Interactions Based on Potential Flow. In Proceedings of the 4th International Conference on Ship Manoeuvring in Shallow and Confined Water, Hamburg, Germany, 23–25 May 2016; pp. 157–167.
20. Todd, F.H. *Series 60 Methodical Experiments with Models of Single-Screw Merchant Ships*; Technical Report 1712; David Taylor Model Basin: Bethesda, MD, USA, 1963.
21. Kriebel, D.; Seelig, W.; Judge, C. Development of a Unified Description of Ship-Generated Waves. In Proceedings of the U.S. Section PIANC Annual Meeting, Roundtable, and Technical Workshops, PIANC USA, Alexandria, VA, USA, 30 June 2003.